Palaeogeography, Palaeoclimatology, Palaeoecology 369 (2013) 422–429

Contents lists available at SciVerse ScienceDirect

Palaeogeography, Palaeoclimatology, Palaeoecology

journal homepage: www.elsevier.com/locate/palaeo

Mid-Holocene East Asian summer monsoon strengthening: Insights from Paleoclimate Modeling Intercomparison Project (PMIP) simulations

Dabang Jiang [a,b,c,*], Xianmei Lang [d], Zhiping Tian [a,e], Lixia Ju [a,c]

[a] Nansen-Zhu International Research Centre, Institute of Atmospheric Physics, Chinese Academy of Sciences, Beijing 100029, China
[b] Key Laboratory of Regional Climate–Environment Research for Temperate East Asia, Chinese Academy of Sciences, Beijing 100029, China
[c] Climate Change Research Center, Chinese Academy of Sciences, Beijing 100029, China
[d] International Center for Climate and Environment Sciences, Institute of Atmospheric Physics, Chinese Academy of Sciences, Beijing 100029, China
[e] University of Chinese Academy of Sciences, Beijing 100049, China

ARTICLE INFO

Article history:
Received 17 April 2012
Received in revised form 6 November 2012
Accepted 8 November 2012
Available online 15 November 2012

Keywords:
Mid-Holocene
East Asian summer monsoon
PMIP models

ABSTRACT

The East Asian summer (June–July–August) monsoon (EASM) is typically thought to have been stronger during interglacial periods based on spatially sparse proxy data. On a large scale, however, whether this view is true and if so, its underlying dynamic mechanisms remain unclear. Using all pertinent experiments within the Paleoclimate Modeling Intercomparison Project (PMIP), here we present an analysis of the EASM during the mid-Holocene, 6000 years ago. Supporting the paleodata, the mid-Holocene EASM, as measured by regionally averaged meridional wind at 850 hPa, became stronger than the baseline period in 27 out of 28 PMIP models with a demonstrable ability to simulate the modern EASM climatology. On average, the EASM strengthened by 32% across all the models and by a larger magnitude in 23 coupled models (35%) than in five atmospheric models (20%). It is proposed that an enhanced land–sea thermal contrast, and hence sea level pressure gradient, between the East Asian continent and adjacent oceans as a result of orbital forcing was responsible for the EASM strengthening during the mid-Holocene.

1. Introduction

The East Asian monsoon is composed of tropical and subtropical monsoons and features southerly winds during summer (June–July–August) and northerly winds during winter (December–January–February) in the lower troposphere (e.g., Tao and Chen, 1987; Ding, 1994). Usually, its intensity in meridional winds has been inferred to become stronger in summer but weaker in winter during interglacial periods of the Quaternary, which is speculated to result from changes in global ice volume and/or orbitally induced solar insolation changes (e.g., Liu and Ding, 1998; Jian et al., 2001; Wang et al., 2008a; Cheng et al., 2009; Wang, 2009). At the East Asian scale, however, whether this interpretation of extremely sparse proxy data is correct remains unclear. And if it is true, the underlying dynamic mechanism remains unidentified.

The mid-Holocene provides a good opportunity for examining how the East Asian monsoon responds to changes of ~5% in the seasonal distribution of the incoming solar radiation at the top of the atmosphere in the Northern and Southern Hemispheres (Berger, 1978). Based on the previous experiments of individual climate models, the mid-Holocene East Asian summer monsoon (EASM) appeared to have been stronger overall during the mid-Holocene (e.g., Wang, 1999, 2000; Chen et al., 2002; Marzin and Braconnot, 2009; Zhou and Zhao, 2009, 2010; Liu et al., 2010). Similar results came from the part of the Paleoclimate Modeling Intercomparison Project (PMIP) simulations (Wang et al., 2010; Zhao and Harrison, 2012). On the other hand, however, there is a large degree of model-dependent uncertainties in both the spatial pattern and magnitude of the mid-Holocene EASM changes among those studies. For example, significant changes in the large-scale EASM circulation during that period were registered only over eastern China north of 30°N in the experiments using a regional climate model (Liu et al., 2010) but over the whole of eastern China in the experiments using a coupled climate model (Marzin and Braconnot, 2009). In addition, whether those climate models can reliably reproduce the present EASM remains unknown, although it is directly related to the confidence of the results. As a matter of fact, it has been revealed that some of the PMIP models failed to describe the present climatological EASM circulation (Jiang and Lang, 2010; see Section 2.2 of this study). Using such models to address the EASM may give wrong conclusions. Furthermore, ocean dynamics has been regarded as a key component in the mid-Holocene climate system (e.g., Braconnot et al., 2007; Ohgaito and Abe-Ouchi, 2009). However, it was not taken into account in most of the earlier experiments with atmospheric models, which may hamper our understanding of the mid-Holocene EASM.

Recently, the mid-Holocene East Asian summer climate was examined using 12 coupled atmosphere–ocean general circulation models (AOGCMs) within the PMIP phase two (PMIP2), and the EASM was

* Corresponding author at: Nansen-Zhu International Research Centre, Institute of Atmospheric Physics, Chinese Academy of Sciences, Beijing 100029, China.
E-mail address: jiangdb@mail.iap.ac.cn (D. Jiang).

0031-0182/$ – see front matter © 2012 Elsevier B.V. All rights reserved.
http://dx.doi.org/10.1016/j.palaeo.2012.11.007

Table 1
Basic information for the 51 PMIP models, together with SCCs and CRMSEs (units: m s^{-1}) of summer meridional wind at 850 hPa between each baseline simulation and the NCEP–NCAR reanalysis data for the period 1981–2000 (Kalnay et al., 1996) within the region of 20°–45°N and 105°–135°E. The 28 models that had positive SCC values statistically significant at the 95% confidence level (Model ID shown in boldface) were chosen for analysis in this study. N/A, not available.

Model ID		Project	Atmospheric resolution	Length of run analyzed (year)	SCC	CRMSE
01	CCC2.0	PMIP1 (AGCM)	T32L10	10	0.07	1.58
02	CCM3	PMIP1 (AGCM)	T42L18	8	0.23	1.46
03	**CCSR1**	PMIP1 (AGCM)	T21L20	10	0.32	1.10
04	CNRM-2	PMIP1 (AGCM)	T31L19	10	0.14	1.52
05	CSIRO	PMIP1 (AGCM)	R21L9	15	0.02	1.17
06	**ECHAM3**	PMIP1 (AGCM)	T42L19	10	0.67	0.75
07	**GEN2**	PMIP1 (AGCM)	T31L18	10	0.56	0.86
08	GFDL	PMIP1 (AGCM)	R30L20	25	−0.24	1.82
09	GISS-IIP	PMIP1 (AGCM)	72×46, L9	10	−0.16	1.80
10	**LMCELMD4**	PMIP1 (AGCM)	48×36, L11	15	0.30	2.14
11	**LMCELMD5**	PMIP1 (AGCM)	64×50, L11	15	0.30	1.24
12	MRI2	PMIP1 (AGCM)	72×46, L15	10	−0.43	2.57
13	UGAMP	PMIP1 (AGCM)	T42L19	20	0.01	1.95
14	UIUC11	PMIP1 (AGCM)	72×46, L14	10	−0.42	1.63
15	UKMO	PMIP1 (AGCM)	96×73, L19	50	−0.28	1.54
16	YONU	PMIP1 (AGCM)	72×46, L7	10	−0.72	2.30
17	**CCSM3.0**	PMIP2 (AOGCM)	T42L18	50	0.70	0.81
18	CSIRO-Mk3L-1.0	PMIP2 (AOGCM)	R21L18	1000	−0.30	1.48
19	CSIRO-Mk3L-1.1	PMIP2 (AOGCM)	R21L18	1000	−0.19	1.34
20	ECBILTCLIOVECODE	PMIP2 (AOGCM)	T21L3	100	N/A	N/A
21	ECHAME5-MPIOM1	PMIP2 (AOGCM)	T31L20	100	0.11	1.16
22	ECHAM53-MPIOM127-LPJ	PMIP2 (AOGCM)	T31L19	100	0.22	1.06
23	FGOALS-1.0 g	PMIP2 (AOGCM)	R42L9	100	0.06	2.48
24	FOAM	PMIP2 (AOGCM)	R15L18	100	−0.26	1.79
25	**GISSmodelE**	PMIP2 (AOGCM)	72×46, L17	50	0.70	0.84
26	**IPSL-CM4-V1-MR**	PMIP2 (AOGCM)	96×72, L19	100	0.72	1.01
27	**MIROC3.2**	PMIP2 (AOGCM)	T42L20	100	0.57	1.34
28	**MRI-CGCM2.3.4fa**	PMIP2 (AOGCM)	T42L30	150	0.33	1.07
29	**MRI-CGCM2.3.4nfa**	PMIP2 (AOGCM)	T42L30	150	0.81	0.57
30	**UBRIS-HadCM3M2**	PMIP2 (AOGCM)	96×73, L19	100	0.46	1.26
31	ECBILTCLIOVECODE-veg	PMIP2 (AOVGCM)	T21L3	100	N/A	N/A
32	ECHAM53-MPIOM127-LPJ-veg	PMIP2 (AOVGCM)	T31L19	100	0.20	1.07
33	FOAM-veg	PMIP2 (AOVGCM)	R15L18	100	−0.28	1.80
34	**MRI-CGCM2.3.4fa-veg**	PMIP2 (AOVGCM)	T42L30	100	0.36	0.95
35	**MRI-CGCM2.3.4nfa-veg**	PMIP2 (AOVGCM)	T42L30	100	0.85	0.48
36	**UBRIS-HadCM3M2-veg**	PMIP2 (AOVGCM)	96×73, L19	100	0.51	1.28
37	**BCC-CSM1.1**	PMIP3 (AOVGCM)	T42L26	100	0.66	0.84
38	**CCSM4**	PMIP3 (AOGCM)	288×192, L26	301	0.52	0.99
39	**CNRM-CM5**	PMIP3 (AOGCM)	256×128, L31	200	0.77	0.73
40	**CSIRO-Mk3-6-0**	PMIP3 (AOGCM)	192×96, L18	100	0.25	1.10
41	CSIRO-Mk3L-1-2	PMIP3 (AOGCM)	64×56, L18	500	−0.25	1.39
42	EC-EARTH-2-2	PMIP3 (AOGCM)	320×160, L62	40	N/A	N/A
43	**FGOALS-g2**	PMIP3 (AOVGCM)	128×60, L26	100	0.80	0.94
44	**FGOALS-s2**	PMIP3 (AOVGCM)	128×108, L26	100	0.31	1.44
45	**GISS-E2-R**	PMIP3 (AOGCM)	144×90, L40	100	0.75	0.78
46	**HadGEM2-CC**	PMIP3 (AOVGCM)	192×145, L60	35	0.79	0.72
47	**HadGEM2-ES**	PMIP3 (AOVGCM)	192×145, L38	102	0.78	0.75
48	**IPSL-CM5A-LR**	PMIP3 (AOVGCM)	96×95, L39	500	0.66	1.11
49	**MIROC-ESM**	PMIP3 (AOVGCM)	T42L80	100	0.43	1.96
50	**MPI-ESM-P**	PMIP3 (AOGCM)	T63L47	100	0.63	0.73
51	**MRI-CGCM3**	PMIP3 (AOGCM)	320×160, L48	100	0.29	1.02

noted to become stronger (Wang et al., 2010). However, no attention was paid in their work to the spatial pattern, magnitude, and dynamic mechanism behind the EASM change during that period. Moreover, they only used some of the PMIP2 AOGCMs, which makes it impossible to evaluate the effect of ocean on the EASM through the comparison of the different types of PMIP simulations. Using 17 atmospheric general circulation models (AGCMs) within the PMIP phase one (PMIP1) and 11 AOGCMs within the PMIP2, Zhao and Harrison (2012) discussed the mid-Holocene EASM through precipitation change. Since precipitation and monsoon relationship in East Asia is not direct as it is in the tropics such as in India (e.g., Tao and Chen, 1987; Ding, 1994), it may be more relevant to directly use low-tropospheric winds instead of precipitation to address the monsoon in East Asia. Again, whether those models can reliably reproduce the modern East Asian climate was neglected in their study. Collectively, all of the aforementioned factors stress the need to specifically examine the mid-Holocene EASM using multiple reliable climate models and estimate the role of interactive ocean therein. Particularly, it is interesting to investigate what the EASM was like during the mid-Holocene in the simulations of state-of-the-art climate models participating in the latest PMIP phase three (PMIP3) under the framework of the Intergovernmental Panel on Climate Change Fifth Assessment Report.

Within the PMIP project, 51 climate models have been used to simulate the mid-Holocene climate to date. Part of the PMIP earlier experiments have improved our knowledge of the mid-Holocene African and Indian tropical monsoon changes (e.g., Joussaume et al., 1999; Braconnot et al., 2002), for example. Given that the mid-Holocene surface air temperature changes over China obtained from the PMIP1 and PMIP2 models agree in general with multi-proxy data during boreal summer, and that the opposite of this situation is true during boreal winter (Jiang et al., 2012), an analysis was made in this study of all available simulations within the PMIP database to examine the mid-Holocene EASM changes, as well as the dynamic mechanisms behind the most common changes.

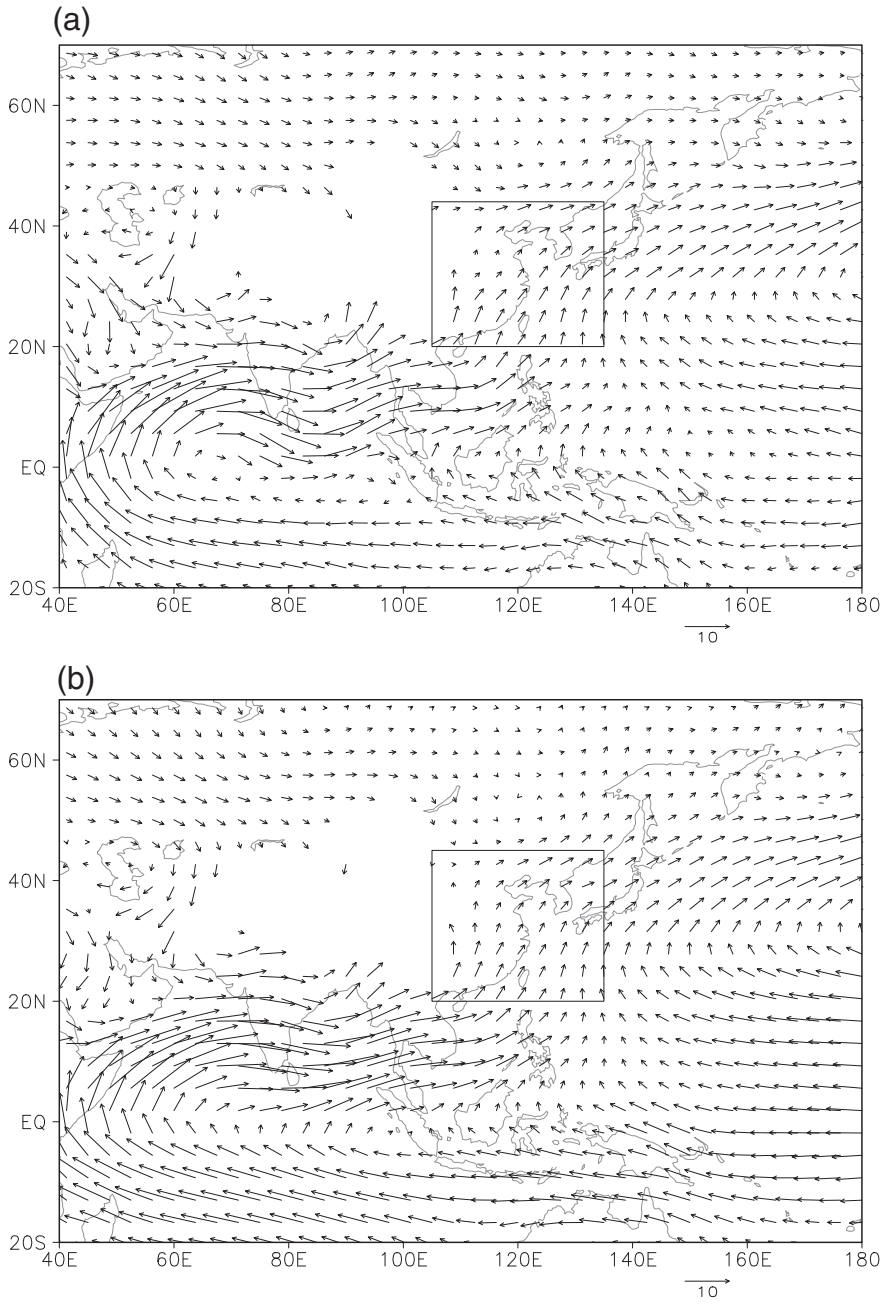

Fig. 1. Climatology of summer wind (units: m s^{-1}) at 850 hPa as derived from (a) the NCEP–NCAR reanalysis data for the period 1981–2000 (Kalnay et al., 1996) and (b) the ensemble mean of the 28 PMIP models for the baseline period, in which regions with an elevation above 1500 m are left blank, and the rectangle shows the region of 20°–45°N and 105°–135°E.

2. Data

2.1. Models and data

This study was based on all of the PMIP experiments for the mid-Holocene climate involving 16 AGCMs from the PMIP1, 14 AOGCMs plus six coupled atmosphere–ocean–vegetation general circulation models (AOVGCMs) from the PMIP2, and eight AOGCMs plus seven AOVGCMs from the PMIP3 (Table 1). Hereafter, AOGCMs and AOVGCMs are referred to as CGCMs. In brief, for the mid-Holocene the most important forcing in the Northern (Southern) Hemisphere was a stronger (weaker) seasonality of insolation, by about 5%, due to the precessional cycle (Berger, 1978). Additional negative forcing was derived from changes in atmospheric concentrations of carbon dioxide from 345 ppm for the present period to 280 ppm for the mid-Holocene in the PMIP1 and of methane from 760 ppb for the pre-industrial period to 650 ppb for the mid-Holocene in the PMIP2. In the PMIP3, concentrations of atmospheric carbon dioxide, methane, and nitrous oxide varied from the pre-industrial levels of 284 ppm, 791 ppb, and 275 ppb to 280 ppm, 650 ppb, and 270 ppb during the mid-Holocene, respectively. Sea surface temperatures (SSTs) were fixed as the present day values in the PMIP1 AGCMs but were computed by oceanic general circulation models in the PMIP2 and PMIP3 CGCMs. In addition, there was a difference in the baseline or reference period for the mid-Holocene climate simulations. The modern period ca. 1950 was used in the PMIP1 AGCM experiments, while the pre-industrial period

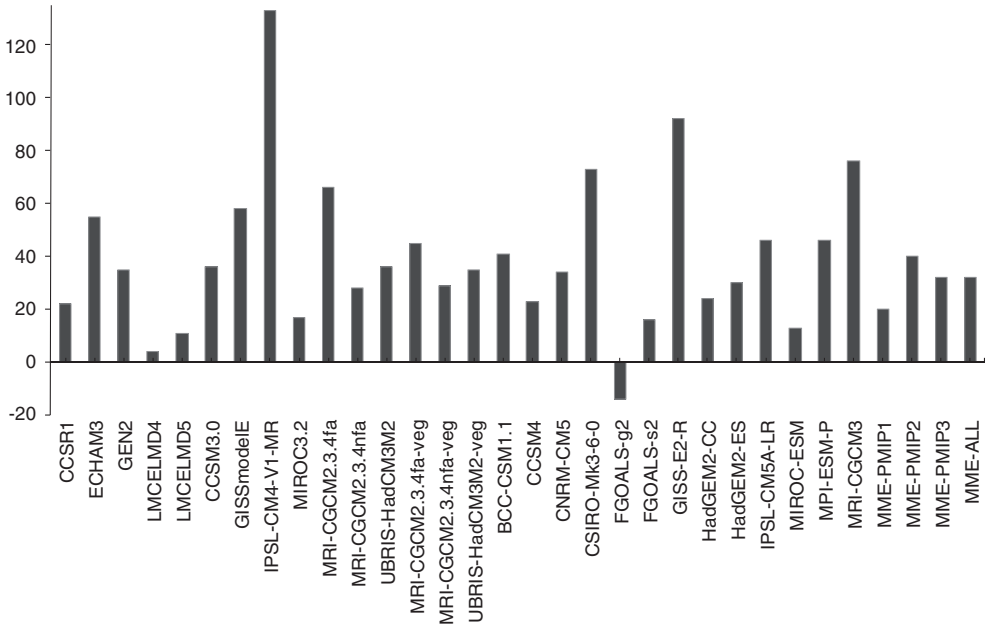

Fig. 2. Percentage changes in the mid-Holocene EASM intensity, which was calculated by regionally averaged meridional wind speed at 850 hPa, with reference to the baseline period as simulated by the 28 PMIP models. MME-PMIP1, MME-PMIP2, MME-PMIP3, and MME-ALL denote the ensemble mean of the five PMIP1 AGCMs, 10 PMIP2 CGCMs, 13 PMIP3 CGCMs, and all the 28 models, respectively.

ca. 1750 was used in the PMIP2 and PMIP3 CGCM experiments. Basic information on those 51 models has been provided in Table 1. Further details, as well as information on boundary conditions and experimental designs, were given by Joussaume and Taylor (1995) and Braconnot et al. (2007), and are available online at http://pmip3.lsce.ipsl.fr/.

2.2. Evaluation of the models

It is well known that, during summer, a low-pressure system dominates over the East Asian continent, while a high-pressure system dominates over the western North Pacific, as a consequence of the difference in thermal capacity between land and ocean. That sea level pressure pattern leads to prevailing southerly winds in the lower troposphere over the East Asian continent (Tao and Chen, 1987; Ding, 1994). Accordingly, low-tropospheric meridional winds are the most important characteristics of the summer monsoon circulation in East Asia. To evaluate the ability of the models to reproduce the modern EASM climatology, spatial correlation coefficients (SCCs) and centered root-mean-square errors (CRMSEs) of meridional wind at 850 hPa between each baseline simulation and the NCEP–NCAR reanalysis data for the period 1981–2000 (Kalnay et al., 1996) were calculated on the basis of 63 grid points within the region of 20°–45°N and 105°–135°E.

As shown in Table 1, SCCs varied from −0.72 (YONU) to 0.85 (MRI-CGCM2.3.4nfa-veg), and CRMSEs varied from 0.48 m s^{-1} (MRI-CGCM2.3.4nfa-veg) to 2.57 m s^{-1} (MRI2). There was a large spread among the models and an overall better performance for the PMIP3 models compared to the previous generation of climate models. Since some models failed to simulate the modern EASM, it was necessary to exclude those unreliable models from the present study. As such, two preconditions were arbitrarily set to identify reliable models. First, the SCC had to be positive; second, it had to be statistically significant at the 95% confidence level. In this manner, 28 models were finally chosen for analysis (see Table 1). Fig. 1 shows clearly that the 28-model ensemble mean with the same weights reproduced large-scale southerly winds at 850 hPa in East Asia reasonably well. Quantitatively, it gave an SCC of 0.88 and a CRMSE of 0.44 m s^{-1}, and hence had a higher reliability than all of the individual models. The ensemble mean of the results of the 28 models were therefore emphasized in our analysis.

3. Results

Given that there is a complex relationship between summer precipitation and monsoon circulation in East Asia (e.g., Wang et al., 2008b), and that we do not know whether the modern relationship between each other is still valid during the mid-Holocene, it should be more reasonable to gauge the EASM strength through low-level wind speeds rather than precipitation for that period. According to the more recent spatial pattern of the EASM configuration (Fig. 1), regionally averaged summer meridional wind at 850 hPa within the region of 20°–45°N and 105°–135°E was directly used to define the large-scale intensity of the EASM in this study. Note that the same or similar indices have been used to examine the modern and past East Asian monsoon changes (e.g., Wang et al., 2008b; Jiang and Lang, 2010).

Based on the records of marine sediments from South China Sea (e.g., Jian et al., 2001), speleothem records in central China (e.g., Wang et al., 2005, 2008a), loess–paleosol sequences in the Chinese Loess Plateau (e.g., Feng et al., 2006), lacustrine sediments in eastern China (e.g., Sun et al., 2009; Li et al., 2011; Zhai et al., 2011; Wu et al., 2012), and so on, the mid-Holocene EASM strength is generally inferred to be stronger than the present day. Consistent with the understanding of the proxy data, 27 out of the 28 PMIP models reproduced a stronger than baseline EASM during the mid-Holocene (Fig. 2), with a range of levels from 4% (LMCELMD4) to 133% (IPSL-CM4-V1-MR). Conversely, the mid-Holocene EASM weakened by 14% in FGOALS-g2, in which anomalous southerly winds occurred in eastern China but anomalous northerly winds occurred in the adjacent ocean. With reference to the baseline period, the mid-Holocene EASM strengthened on average by 32% for all the models. The 28-model ensemble mean of the mid-Holocene minus baseline differences was characterized by southerly winds at 850 hPa over East Asia, which was in line with the baseline southerly winds in the lower troposphere (Figs. 3a and 1b). Such a systematic strengthening of the mid-Holocene EASM was further demonstrated in Fig. 3b, in which zonally averaged meridional wind anomalies at 850 hPa within 105°–135°E were uniformly above the baseline values over East Asia across 27 of the 28 models (excluding FGOALS-g2) and the 28-model ensemble mean. Therefore, there was a robust qualitative consistency on the mid-Holocene EASM strengthening among the PMIP models, although there was a degree

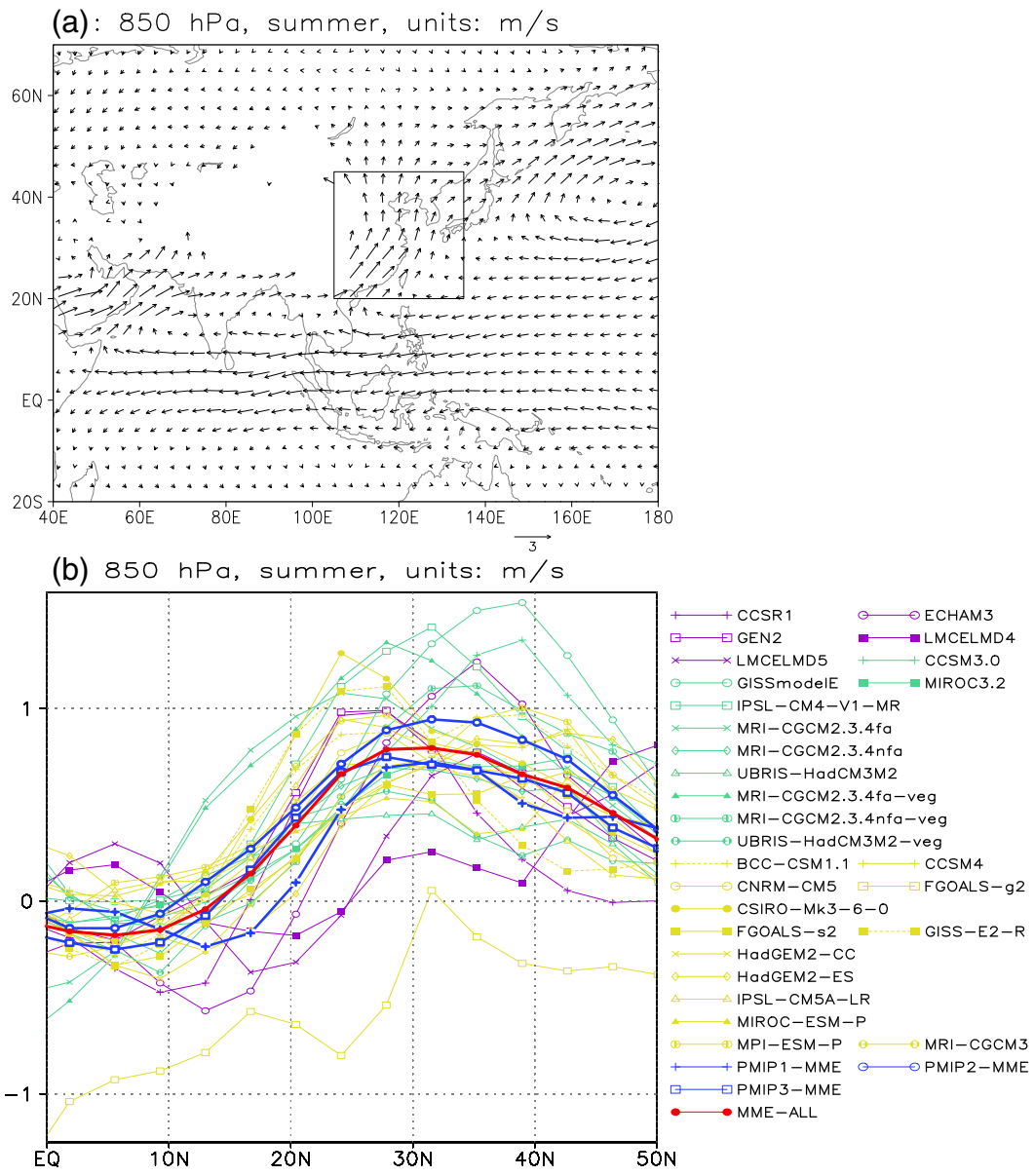

Fig. 3. (a) Mid-Holocene minus baseline differences in wind as derived from the ensemble mean of the 28 PMIP models, in which regions with an elevation above 1500 m are left blank, and the rectangle shows the region of 20°–45°N and 105°–135°E. (b) Mid-Holocene minus baseline differences in meridional wind zonally averaged within 105°–135°E. Northward wind speed is positive.

of model-dependent uncertainty in the magnitude and a weakening in FGOALS-g2. The underlying dynamic mechanisms were as follows.

In response to the mid-Holocene changes in the Earth's orbital parameters and atmospheric concentrations of carbon dioxide in the PMIP1, methane in the PMIP2, and carbon dioxide, methane, and nitrous oxide in the PMIP3 (see Section 2.1), summer surface temperature rose significantly over the East Asian continent but changed only slightly over the adjacent oceans for the PMIP models as a whole (Fig. 4a). Such changes led to a strengthened zonal land–sea thermal contrast between the East Asian continent and the western North Pacific during the mid-Holocene (Fig. 5a). Quantitatively, the difference in regionally averaged summer surface temperature between 90°–135°E and 135°E–180° within 10°–50°N was enhanced by 0.56 K for the 28-model ensemble mean. In turn, summer sea level pressure reduced over the East Asian continent (Fig. 4b), which strengthened the Asian low-pressure system. On the contrary, it rose over the North Pacific, which strengthened the subtropical high-pressure system over the western North Pacific. Both the changes led to an increased zonal gradient of summer sea level pressure from the western North Pacific through the East Asian continent. Taken together, those increased zonal land–sea thermal contrast and zonal sea level pressure gradient gave rise finally to a systematic strengthening of the mid-Holocene EASM circulation in the lower troposphere in terms of the dynamic mechanism for the formation of the EASM (e.g., Tao and Chen, 1987; Ding, 1994). Based on the above, it should be noted that the mid-Holocene EASM strengthening also can be obtained through the traditional EASM index defined by a zonal sea level pressure difference between the western North Pacific and the East Asian continent (e.g., Guo et al., 2003; Wang et al., 2008b).

At the same time, surface temperature elevated over the East Asian continent but reduced slightly over the South China Sea during the mid-Holocene (Figs. 4a and 5b). Moreover, surface temperature warming was stronger overall in the north than in the south over the East Asian continent. As a result, meridional thermal contrast increased through the South China Sea to the high latitude areas of

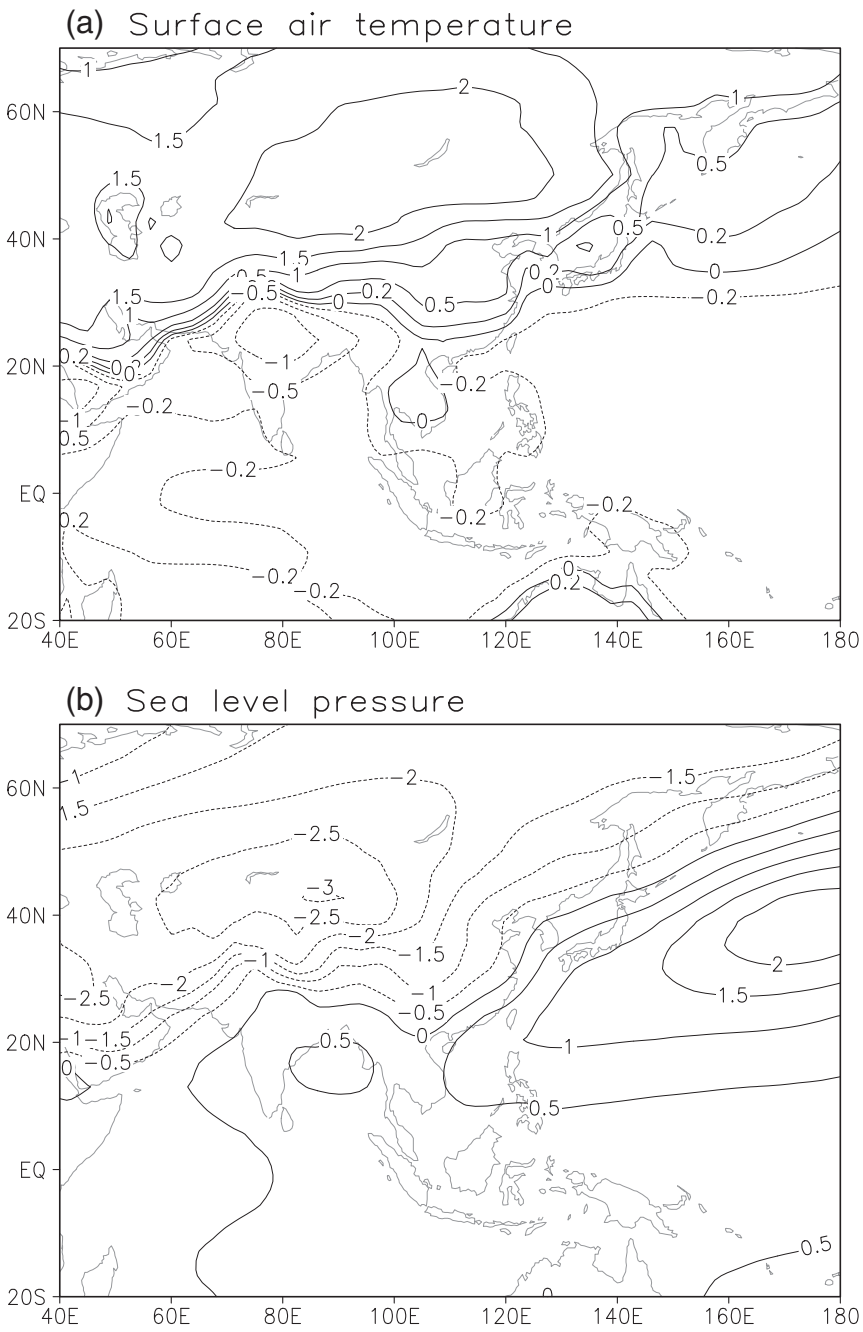

Fig. 4. Mid-Holocene minus baseline differences in summer (a) surface air temperature (units: K) and (b) sea level pressure (units: hPa) from the ensemble mean of the 28 PMIP models.

East Asia. Anomalous southerly winds were consequently induced in the lower troposphere over East Asia, and they were used to compensate atmospheric mass loss due to an intensified ascending motion in the mid- and high latitudes of East Asia. In this way, the EASM was further strengthened during the mid-Holocene.

There is a debate about the ocean influence on the Asian monsoon climate during the mid-Holocene (Liu et al., 2004; Zhao and Harrison, 2012). More specifically, both negative and positive effects of the interactive ocean on the mid-Holocene EASM were derived from the earlier simulations of individual models (Wei and Wang, 2004; Marzin and Braconnot, 2009). Within the PMIP project, as discussed by Braconnot et al. (2007), ocean dynamics were included in the CGCMs but were neglected in the AGCMs, allowing for a preliminary investigation of the role of interactive ocean. When viewed in terms of these two kinds of climate models, the mid-Holocene EASM strengthened on average by 20% in the five PMIP1 AGCMs, by 40% in the 10 PMIP2 CGCMs, and by 32% in the 13 PMIP3 CGCMs (Fig. 2). A strengthening of 35% was obtained from the 23 PMIP2 and PMIP3 CGCMs. As a whole, the CGCMs yielded an EASM much stronger than that from the AGCMs, which was due largely to the major role played by the computed SSTs. Excluding CCSM4, FGOALS-g2, FGOALS-s2, and MIROC-ESM in which SST data are not yet available, 17 out of the 19 PMIP2 and PMIP3 CGCMs were found to reproduce overall colder than baseline SSTs in the oceans adjacent to the East Asian continent, which resulted from the latitudinal gradient in the insolation forcing and the thermal inertia of the ocean as detailed by Marzin and Braconnot (2009). This state was also appropriate for the ensemble mean of the 19 CGCMs (Fig. 6). For example, regionally averaged SSTs within 0°–40°N and 105°E–180° varied from −0.65 K (GISS-E2-R) to 0.14 K (HadGEM2-ES) and decreased by an average of 0.26 K across

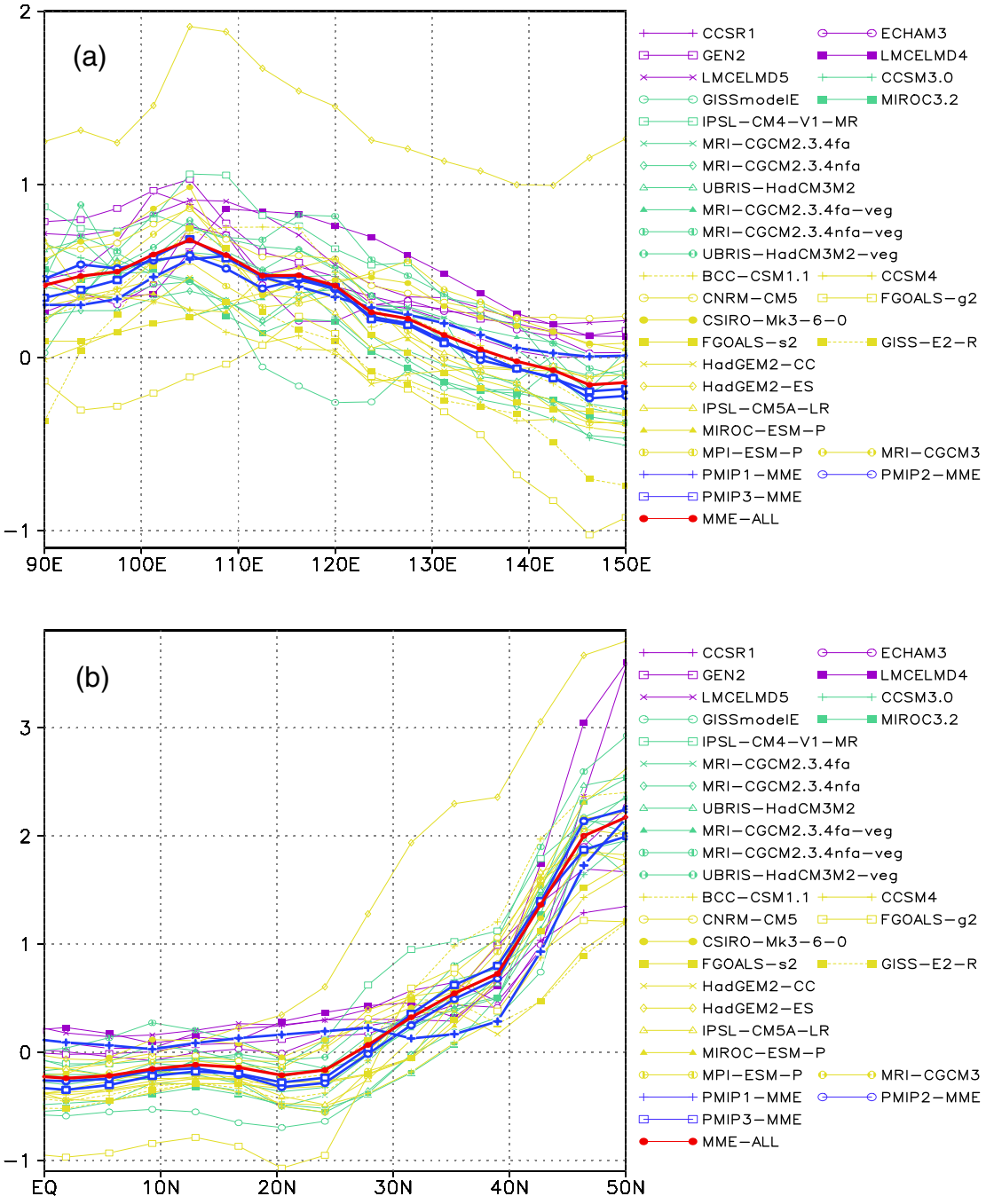

Fig. 5. Mid-Holocene minus baseline differences in summer surface air temperature (units: K), (a) longitudinally averaged within 10°–50°N, and (b) zonally averaged within 105°–135°E.

the 19 CGCMs. In contrast, SSTs were fixed as the modern values in the AGCM experiments. In this situation, combined with changes in surface temperature over East Asia, the simulated difference of the mid-Holocene summer thermal contrast between the East Asian continent and the adjacent western North Pacific was larger in the CGCMs than in the AGCMs (Fig. 5a). In quantitative terms, the zonal difference in regionally averaged summer surface temperature between 90°–135°E and 135°E–180° within 10°–50°N increased on average by 0.58 K for the 23 PMIP2 and PMIP3 CGCMs, which was larger than the 0.48 K derived from the five AGCMs during the mid-Holocene. Accordingly, the strengthening of the mid-Holocene EASM was greater in the former than in the latter. That is, interactive ocean amplified the orbitally forced EASM enhancement during the mid-Holocene. Note that part of the aforementioned differences in the mid-Holocene EASM change between the PMIP AGCM and CGCM simulations were probably due to the differences in climate models and experimental designs. To detect ocean feedback more directly, the control experiments of coupled models would be the reference for the mid-Holocene experiments either with the coupled model or with the atmosphere-only model alone for the same climate model system (e.g., Marzin and Braconnot, 2009).

4. Conclusion

The present analysis provided a clear picture of the mid-Holocene EASM change and the underlying dynamic mechanism from the perspective of multiple climate models within the PMIP project. Twenty-seven out of the 28 PMIP models simulated a stronger than

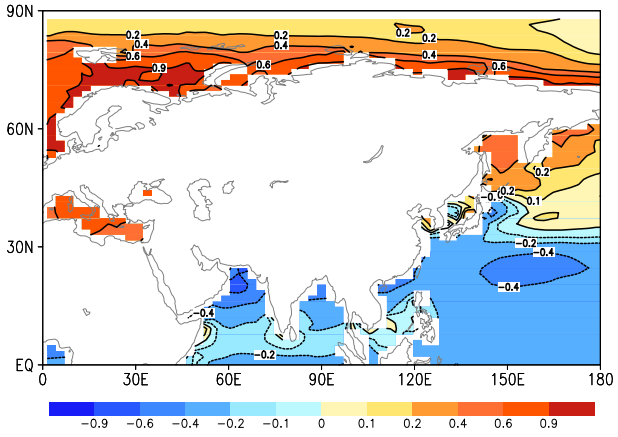

Fig. 6. Mid-Holocene minus baseline differences in summer SSTs (units: K) as derived from the ensemble mean of the 10 PMIP2 CGCMs plus nine PMIP3 CGCMs (excluding CCSM4, FGOALS-g2, FGOALS-s2, and MIROC-ESM in which SST data are not available).

baseline EASM during that period. On average, the mid-Holocene EASM intensity increased by 32% relative to the baseline level. Changes in zonal and meridional surface temperature contrasts, and hence sea level pressure gradients, across the regions of concern were responsible for the mid-Holocene EASM strengthening. More of the strengthening in the CGCMs, with reference to the AGCMs with fixed modern SSTs, was related to the effect of interactive ocean.

Acknowledgments

We sincerely thank Prof. Peter Kershaw and the anonymous reviewer for their helpful comments on the manuscript, and thank Joyce Bosmans, Pascale Braconnot, Johann Jungclaus, Akio Kitoh, Allegra N. LeGrande, Charline Marzin, Rumi Ohgaito, Bette L. Otto-Bliesner, Steven J. Phipps, Leon Rotstayn, Stéphane Sénési, Tongwen Wu, and Tianjun Zhou for providing information on the PMIP3 models. Also, we acknowledge the international modeling groups for providing their data for analysis, and the Laboratoire des Sciences du Climat et de l'Environnement (LSCE) for collecting and archiving the model data. This research was supported by the Strategic Priority Research Program (XDA05120703 and XDB03020600) and the Knowledge Innovation Program (KZCX2-EW-QN202) of the Chinese Academy of Sciences and by the National Natural Science Foundation of China (41222034, 41175072, and 40805030). The PMIP2/MOTIF Data Archive is supported by CEA, CNRS, the EU project MOTIF (EVK2-CT-2002-00153) and the Programme National d'Etude de la Dynamique du Climat (PNEDC). The analyses were performed using version 31 October 2012 of the PMIP phases one to three databases. More information is available on http://motif.lsce.ipsl.fr/, http://pmip2.lsce.ipsl.fr/, and http://pmip3.lsce.ipsl.fr/.

References

Berger, A.L., 1978. Long-term variations of daily insolation and Quaternary climatic changes. Journal of the Atmospheric Sciences 35, 2362–2367.
Braconnot, P., Loutre, M.-F., Dong, B., Joussaume, S., Valdes, P., PMIP participating groups, 2002. How the simulated change in monsoon at 6 ka BP is related to the simulation of the modern climate: results from the Paleoclimate Modeling Intercomparison Project. Climate Dynamics 19, 107–121.
Braconnot, P., Otto-Bliesner, B., Harrison, S., Joussaume, S., Peterchmitt, J.-Y., Abe-Ouchi, A., Crucifix, M., Driesschaert, E., Fichefet, Th., Hewitt, C.D., Kageyama, M., Kitoh, A., Laîné, A., Loutre, M.-F., Marti, O., Merkel, U., Ramstein, G., Valdes, P., Weber, S.L., Yu, Y., Zhao, Y., 2007. Results of PMIP2 coupled simulations of the mid-Holocene and Last Glacial Maximum — part 1: experiments and large-scale features. Climate of the Past 3, 261–277.
Chen, X., Yu, G., Liu, J., 2002. Mid-Holocene climate simulation and discussion on the mechanism of temperature changes in eastern Asia (in Chinese). Science in China Series D: Earth Sciences 32, 335–345.
Cheng, H., Edwards, R.L., Broecker, W.S., Denton, G.H., Kong, X., Wang, Y., Zhang, R., Wang, X., 2009. Ice age terminations. Science 326, 248–252.
Ding, Y.H., 1994. Monsoons Over China. Springer, pp. 1–419.
Feng, Z.-D., Tang, L.Y., Wang, H.B., Ma, Y.Z., Liu, K.-B., 2006. Holocene vegetation variations and the associated environmental changes in the western part of the Chinese Loess Plateau. Palaeogeography, Palaeoclimatology, Palaeoecology 241, 440–456.
Guo, Q.Y., Cai, J.N., Shao, X.M., Sha, W.Y., 2003. Interdecadal variability of East-Asian summer monsoon and its impact on the climate of China. Acta Geographica Sinica 58, 569–576.
Jian, Z., Huang, B., Kuhnt, W., Lin, H.-L., 2001. Late Quaternary upwelling intensity and East Asian monsoon forcing in the South China Sea. Quaternary Research 55, 363–370.
Jiang, D., Lang, X., 2010. Last Glacial Maximum East Asian monsoon: results of PMIP simulations. Journal of Climate 23, 5030–5038.
Jiang, D., Lang, X., Tian, Z., Wang, T., 2012. Considerable model-data mismatch in temperature over China during the mid-Holocene: results of PMIP simulations. Journal of Climate 25, 4135–4153.
Joussaume, S., Taylor, K.E., 1995. Status of the Paleoclimate Modeling Intercomparison Project (PMIP). In: Gates, W.L. (Ed.), Proceedings of the First International AMIP Scientific Conference. World Meteorol. Org., Geneva, pp. 425–430 (WCRP-92, WMO/TD-732).
Joussaume, S., Taylor, K.E., Braconnot, P., Mitchell, J.F.B., Kutzbach, J.E., Harrison, S.P., Prentice, I.C., Broccoli, A.J., Abe-Ouchi, A., Bartlein, P.J., Bonfils, C., Dong, B., Guiot, J., Herterich, K., Hewitt, C.D., Jolly, D., Kim, J.W., Kislov, A., Kitoh, A., Loutre, M.F., Masson, V., McAvaney, B., McFarlane, N., de Noblet, N., Peltier, W.R., Peterschmitt, J.Y., Pollard, D., Rind, D., Royer, J.F., Schlesinger, M.E., Syktus, J., Thompson, S., Valdes, P., Vettoretti, G., Webb, R.S., Wyputta, U., 1999. Monsoon changes for 6000 years ago: results of 18 simulations from the Paleoclimate Modeling Intercomparison Project (PMIP). Geophysical Research Letters 26, 859–862.
Kalnay, E., Kanamitsu, M., Kistler, R., Collins, W., Deaven, D., Gandin, L., Iredell, M., Saha, S., White, G., Woollen, J., Zhu, Y., Chelliah, M., Ebisuzaki, W., Higgins, W., Janowiak, J., Mo, K.C., Ropelewski, C., Wang, J., Leetmaa, A., Reynolds, R., Jenne, R., Joseph, D., 1996. The NCEP/NCAR reanalysis project. Bulletin of the American Meteorological Society 77, 437–472.
Li, C., Wu, Y., Hou, X., 2011. Holocene vegetation and climate in Northeast China revealed from Jingbo Lake sediment. Quaternary International 229, 67–73.
Liu, T.S., Ding, Z.L., 1998. Chinese loess and the paleomonsoon. Annual Review of Earth and Planetary Sciences 26, 111–145.
Liu, Z., Harrison, S.P., Kutzbach, J., Otto-Bliesner, B., 2004. Global monsoons in the mid-Holocene and oceanic feedback. Climate Dynamics 22, 157–182.
Liu, Y., He, J., Li, W., Chen, L., Li, W., Zhang, B., 2010. MM5 simulations of the China regional climate during the mid-Holocene. Acta Meteorologica Sinica 24, 468–483.
Marzin, C., Braconnot, P., 2009. The role of the ocean feedback on Asian and African monsoon variations at 6 kyr and 9.5 kyr BP. Comptes Rendus Geosciences 341, 643–655.
Ohgaito, R., Abe-Ouchi, A., 2009. The effect of sea surface temperature bias in the PMIP2 AOGCMs on mid-Holocene Asian monsoon enhancement. Climate Dynamics 33, 975–983.
Sun, Q., Wang, S., Zhou, J., Shen, J., Cheng, P., Xie, X., Wu, F., 2009. Lake surface fluctuations since the late glaciation at Lake Daihai, North central China: a direct indicator of hydrological process response to East Asian monsoon climate. Quaternary International 194, 45–54.
Tao, S.Y., Chen, L.X., 1987. A review of recent research on the East Asian monsoon in China. In: Chang, C.-P., Krishnamurti, T.N. (Eds.), Monsoon Meteorology. Oxford University Press, pp. 60–92.
Wang, H.J., 1999. Role of vegetation and soil in the Holocene megathermal climate over China. Journal of Geophysical Research 104 (D8), 9361–9367.
Wang, H.J., 2000. The seasonal climate and low frequency oscillation in the simulated mid-Holocene megathermal climate. Advances in Atmospheric Sciences 17, 445–457.
Wang, P.X., 2009. Global monsoon in a geological perspective. Chinese Science Bulletin 54, 1113–1136.
Wang, Y., Cheng, H., Edwards, R.L., He, Y., Kong, X., An, Z., Wu, J., Kelly, M.J., Dykoski, C.A., Li, X., 2005. The Holocene Asian monsoon: links to solar changes and North Atlantic climate. Science 308, 854–857.
Wang, Y., Cheng, H., Edwards, R.L., Kong, X., Shao, X., Chen, S., Wu, J., Jiang, X., Wang, X., An, Z., 2008a. Millennial- and orbital-scale changes in the East Asian monsoon over the past 224,000 years. Nature 451, 1090–1093.
Wang, B., Wu, Z., Li, J., Liu, J., Chang, C.-P., Ding, Y., Wu, G., 2008b. How to measure the strength of the East Asian summer monsoon. Journal of Climate 21, 4449–4463.
Wang, T., Wang, H.J., Jiang, D., 2010. Mid-Holocene East Asian summer climate as simulated by the PMIP2 models. Palaeogeography, Palaeoclimatology, Palaeoecology 288, 93–102.
Wei, J.F., Wang, H.J., 2004. A possible role of solar radiation and ocean in the mid-Holocene East Asian monsoon climate. Advances in Atmospheric Sciences 21, 1–12.
Wu, X., Zhang, Z., Xu, X., Shen, J., 2012. Asian summer monsoonal variations during the Holocene revealed by Huguangyan maar lake sediment record. Palaeogeography, Palaeoclimatology, Palaeoecology 323–325, 13–21.
Zhai, D., Xiao, J., Zhou, L., Wen, R., Chang, Z., Wang, X., Jin, X., Pang, Q., Itoh, S., 2011. Holocene East Asian monsoon variation inferred from species assemblage and shell chemistry of the ostracodes from Hulun Lake, Inner Mongolia. Quaternary Research 75, 512–522.
Zhao, Y., Harrison, S.P., 2012. Mid-Holocene monsoons: a multi-model analysis of the inter-hemispheric differences in the responses to orbital forcing and ocean feedbacks. Climate Dynamics 39, 1457–1487.
Zhou, B.T., Zhao, P., 2009. Inverse correlation between ancient winter and summer monsoons in East Asia? Chinese Science Bulletin 54, 3760–3767.
Zhou, B.T., Zhao, P., 2010. Modeling variations of summer upper tropospheric temperature and associated climate over the Asian Pacific region during the mid-Holocene. Journal of Geophysical Research 115, D20109. http://dx.doi.org/10.1029/2010JD014029.